Biomaterials 291 (2022) 121864

Contents lists available at ScienceDirect

Biomaterials

journal homepage: www.elsevier.com/locate/biomaterials

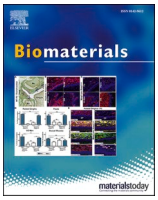

Tuning pro-survival effects of human induced pluripotent stem cell-derived exosomes using elastin-like polypeptides

Chen-Hung Lee [a,**], Daniel Hunt [b], Julien George Roth [c], Ching-Chi Chiu [d], Riley A. Suhar [e], Bauer L. LeSavage [f], Alexis Jane Seymour [f], Chris Lindsay [e], Brad A. Krajina [b], Yi-Tung Chen [g], Kuo-Hsuan Chang [h], I-Chang Hsieh [a], Pao-Hsien Chu [a], Ming-Shien Wen [a], Sarah C. Heilshorn [e,*]

[a] Division of Cardiology, Department of Internal Medicine, Chang Gung Memorial Hospital-Linkou, Chang Gung University College of Medicine, Taoyuan, Taiwan
[b] Department of Chemical Engineering, Stanford University, Stanford, CA, USA
[c] Institute for Stem Cell Biology and Regenerative Medicine, Stanford University, Stanford, CA, USA
[d] Department of Medical Biotechnology and Laboratory Science, College of Medicine, Chang Gung University, Taoyuan, Taiwan
[e] Department of Materials Science & Engineering, Stanford University, Stanford, CA, USA
[f] Department of Bioengineering, Stanford University, Stanford, CA, USA
[g] Molecular Medicine Research Center, Chang Gung University, Taoyuan, 333, Taiwan
[h] Department of Neurology, Chang Gung Memorial Hospital and University School of Medicine, Taiwan

ARTICLE INFO

Keywords:
Elastin-like polypeptides
Human induced pluripotent stem cells
Exosomes
Biomaterials
Recombinant protein
Cell culture coating
Extracellular matrix

ABSTRACT

Exosome-based regenerative therapies are potentially easier to manufacture and safer to apply compared to cell-based therapies. However, many questions remain about how to bio-manufacture reproducible and potent exosomes using animal-free reagents. Here we evaluate the hypothesis that designer biomaterial substrates can be used to alter the potency of exosomes secreted by human induced pluripotent stem cells (iPSCs). Two animal-free designer matrices were fabricated based on recombinant elastin-like polypeptides (ELPs): one including a cell-adhesive RGD ligand and a second with a non-adhesive RDG peptide. While iPSCs cultured on these two substrates and Matrigel-coated controls had similar levels of proliferation, the RDG-ELP substrate significantly increased protein expression of stemness markers OCT4 and SOX2 and suppressed spontaneous differentiation compared to those on RGD-ELP. The pro-survival potency of iPSC-derived exosomes was evaluated using three distinct stress tests: serum starvation in murine fibroblasts, hypoxia in human endothelial cells, and hyper-osmolarity in canine kidney cells. In all three cases, exosomes produced by iPSCs grown on RDG-ELP substrates had similar pro-survival effects to those produced using iPSCs grown on Matrigel, while use of RGD-ELP substrates led to significantly reduced exosome potency. These data demonstrate that recombinant substrates can be designed for the robust bio-manufacturing of iPSC-derived, pro-survival exosomes.

1. Introduction

Stem cells are considered an important cell source for regenerative medicine and have been explored for a wide array of potential therapeutic uses, including treatment of myocardial infarction, retinal diseases, spinal cord injury, wounds, and stroke [1–3]. Human induced pluripotent stem cells (iPSCs), first described in 2007 [4], closely resemble embryonic stem cells (ESCs) [5,6] while overcoming two important obstacles associated with ESCs: immune rejection after transplantation and ethical concerns regarding the use of human embryos [4,7]. Mounting evidence suggests that much of the regenerative capacity of iPSCs lies in their paracrine secretion of extracellular vesicles including exosomes, an extracellular vesicle with an endosomal origin [8,9]. Delivery of iPSC-secreted exosomes, which are typically 30–150 nm in diameter, has emerged as a promising approach to achieve a cell-free alternative to stem cell therapy [10–12]. In some instances,

* Corresponding author. 476 Lomita Mall, McCullough Room 248, Stanford University, Stanford, CA, 94305, USA.
** Corresponding author. Chang Gung University, College of Medicine, Taoyuan, Taiwan.
E-mail addresses: chl5265@gmail.com (C.-H. Lee), hunt.daniel.robert@gmail.com (D. Hunt), jgroth@stanford.edu (J.G. Roth), ccchei@mail.cgu.edu.tw (C.-C. Chiu), nsuhar@stanford.edu (R.A. Suhar), lesavage@stanford.edu (B.L. LeSavage), aseymour@stanford.edu (A.J. Seymour), cdlindsay17@gmail.com (C. Lindsay), bradkrajina@gmail.com (B.A. Krajina), love5p3@yahoo.com.tw (Y.-T. Chen), gophy5128@cgmh.org.tw (K.-H. Chang), hsiehic@ms28.hinet.net (I.-C. Hsieh), taipei.chu@gmail.com (P.-H. Chu), wenms123@cgmh.org.tw (M.-S. Wen), heilshorn@stanford.edu (S.C. Heilshorn).

https://doi.org/10.1016/j.biomaterials.2022.121864
Received 24 May 2022; Received in revised form 3 September 2022; Accepted 17 October 2022
Available online 26 October 2022

stem cell-derived exosome treatment has shown an identical or improved outcome compared to cell-based therapy [13,14]. In general, cell-free therapies are thought to be easier to bio-manufacture and safer for clinical translation compared to cellular therapies [11], which require strict storage and shipping protocols to maintain cell viability and stringent cell characterization methods to avoid potential teratoma formation [15,16].

To accelerate clinical translation of potential exosome therapies, protocols must be developed to ensure the robust bio-manufacturing of potent exosomes without the use of animal-derived reagents, as these materials suffer from variation between batches and potential contamination with animal proteins or pathogens, all of which can lead to unexpected outcomes [17,18]. To this end, we herein evaluate the use of animal-free, designer biomaterials as substrates for iPSC-derived exosome manufacturing. Several biomaterial strategies, including microgrooved culture substrates and combinatorial biopolymer mixtures, have been reported to alter the phenotype of iPSC-derived cells through cell-substrate interactions [19,20]. Thus, we hypothesized that designer biomaterial substrates with different levels of cell-substrate adhesion would alter the potency of human iPSC-derived exosomes. While exosomes are reported to carry a broad range of bioactive cargo molecules and hence can result in diverse physiological effects [21,22], for the purposes of this manuscript we will define "exosome potency" as the ability of exosomes to protect treated cells from death induced by external stressors.

Matrigel is widely used as a scaffold material to maintain stemness in iPSC cultures [23,24], and iPSCs cultured on Matrigel are able to secrete potent exosomes [25,26]. However, the derivation of Matrigel from murine Engelbreth-Holm-Swarm sarcoma cells makes this material unsuitable for clinical applications. Furthermore, Matrigel consists of an irreproducible, complex mixture of biopolymers, with greater than 45% batch-to-batch variability [27,28]. In contrast, elastin-like polypeptides (ELPs), which are recombinant engineered proteins with repetitive amino acid sequences based on human elastin, have exact chemical structures that are precisely dictated by the engineered genetic template [29]. ELPs are a broad class of compatible materials that have been explored in a number of different biomedical applications [30–32].

ELPs are frequently designed to include a cell-adhesive peptide motif, often arginine, glycine, aspartic acid (RGD), to promote binding of cell-surface integrin receptors [33,34]. Integrin heterodimers comprising sub-units α5, α6, α*v*, β1, and β5 are all abundantly expressed by human iPSCs and are known receptors for the RGD ligand [35,36]. Alternatively, non-cell-adhesive variants of ELP are created by simply scrambling the amino acid sequence of the cell-adhesive ligand (RDG) while maintaining the rest of the amino acid sequence intact [37]. We hypothesized that these two substrates (ELP harboring the RGD *vs.* the RDG peptide) would alter iPSC phenotype, and potentially exosome potency, since binding of integrins is known to induce a vast number of structural and signaling changes within cells [38]. By comparing the potency of exosomes produced using these different substrates, we sought to identify a reproducible, animal-free substrate that enables bio-manufacturing of exosomes with similar potency to those produced using Matrigel.

2. Materials and methods

2.1. Protein synthesis and purification

According to a previously published procedure [39,40], BL21(DE3) pLysS *Escherichia coli E. col*) (Life Technologies), having pET15b plasmids harboring recombinant genes encoding ELPs under control of the T7 promoter, were used to express RGD-ELP and RDG-ELP. Terrific Broth was used to grow the *E. coli* to an optical density (OD_{600}) of 0.8, and the expression of ELP was induced by adding 1 mM isopropyl β-D-1-thiogalactopyranoside. Following 7 h, the *E. coli* were collected by centrifugation, resuspended in TEN buffer (pH 8.0, 10 mM Tris, 100 mM NaCl and 1 mM ethylenediaminetetraacetic acid (EDTA)), and lysed by three freeze–thaw cycles. One mM phenylmethanesulfonyl fluoride protease inhibitor and DNAse I were added to the lysates. Inverse temperature cycling and dialysis against deionized water were carried out for purification and desalination of ELPs, respectively. After lyophilization, the ELP appears as a white solid, and protein purity was confirmed by Western blot (Fig. S1A). Purified protein was solubilized in Dulbecco's phosphate buffered saline (DPBS) overnight at 4 °C prior to use. The ELPs have a repeating elastin-like VPGxG sequence, where x is I (isoleucine) in 80% of the repeats, and x is K (lysine) in 20% of the repeats. Fifteen VPGxG repeats were included in a single "elastin-like domain," and four elastin-like domains were interspersed with four fibronectin-derived domains in the full-length ELP. This resulted is a total of 60 VPGxG repeats in each ELP protein. The transition temperature was 32 °C, and plate coatings were performed below the transition temperature [41]. The tag region was not removed for our cell experiments. The two engineered proteins, RDG-ELP and RGD-ELP, were identical in their amino acid content; they simply vary in the order of the two amino acids D and G. Due to this identical amino acid content, the two polymers had identical molecular weight, identical isoelectric point, identical lower critical solution temperature (LCST) behavior, and identical surface coverage properties. Thus, changes in cell behavior on these two substrates can be directly attributed to altered integrin engagement with the RGD ligand [42,43].

2.2. Substrate preparation

Adsorbed substrates (RDG-ELP and RGD-ELP) were prepared on tissue culture plates by dissolving lyophilized protein in DPBS at 1 mg/ml, pipetting these solutions on top of the surfaces, and incubating the samples overnight at 4 °C. Control surfaces were prepared using Matrigel (6 μg/cm^2, BD Biosciences) for 30 min at 37 °C or tissue culture plates without Matrigel coatings. All surfaces were washed thrice with DPBS at room temperature. The amount of adsorbed protein was quantified using a bicinchoninic acid assay (BCA) according to the manufacturer's recommended protocol (Pierce, Rockford, IL, USA). Simultaneously, a set of standard solutions containing known concentrations of the protein of interest were prepared in DPBS (0, 7.5, 15, 30, 60, and 120 μg/ml) and mixed with an equal volume of BCA working reagent. All reaction plates were sealed and incubated for 1 h at 60 °C. The solutions were then equilibrated at room temperature for ~20 min, and absorbance readings were taken at 562 nm (Fig. S1B).

2.3. Culture of iPSCs

Human iPSC lines (SCVI480, 511.3, and IBMS-iPSC-001-02) were obtained from the Stanford Cardiovascular Institute iPSC Biobank (kind gift from Prof. Joseph C. Wu) [44], Prof. Theo Palmer at the Stanford Neurosurgery Department [45], and the Human Disease iPS Cells Service Consortium (Taiwan) [46], respectively. Pluripotency of the iPSCs was previously confirmed by the expression of pluripotency genes and also validated by teratoma formation in NOD-SCID mice [44–46]. The iPSCs were maintained under feeder-free conditions in defined E8 medium (Life Technologies) on tissue culture plates and passaged every 3–4 days in 5% CO_2/5% O_2/90% N_2 environment at 37 °C. Cultures were plated on freshly prepared substrates for all experiments to standardize the procedure.

2.4. Polyethylene glycol (PEG) enrichment of exosomes

Exosomes were purified following a previously reported protocol [47]. Briefly, vesicle-containing medium from cell cultures was centrifuged at 300×*g* for 10 min followed by 2000 ×g for another 10 min and 10,000 ×g for 30 min at 4 °C to remove large apoptotic bodies and cellular debris. After centrifugation, stock solutions of 40 wt% PEG (8000 MW) and 0.5 M NaCl (Sigma-Aldrich) were added to the solution

to achieve a final concentration of 10 wt% PEG and 50 mM NaCl, respectively. Samples were mixed thoroughly by inversion and incubated at 4 °C for at least 14 h. The next day, samples were centrifuged at 10,000 ×g for 60 min at 4 °C. Conical tubes were then decanted and allowed to drain for 5 min, tapping occasionally to remove excess PEG. The resulting pellet was re-suspended in 1 ml DPBS and centrifuged at 110,000 ×g for 2 h to wash and re-pellet the vesicles. Obtained exosome samples were stored at −80 °C until use.

2.5. Exosome characterization

Total protein from the exosome pellet was extracted in Radio-Immune Precipitation Assay (RIPA) lysis buffer (Thermo Fisher Scientific), and protein concentrations were determined with the BCA Protein Assay Kit according to manufacturer's protocol. Samples with equal protein concentrations (20 μg/ml) were boiled at 95 °C for 5 min and loaded onto sodium dodecyl sulfate polyacrylamide gel electrophoresis (SDS-PAGE) (12% separating gel and 5% stacking gel), then transferred to a polyvinylidene difluoride (PVDF) membrane (Thermo). The membranes were blocked with 5% nonfat dry milk and incubated with the primary antibodies overnight at 4 °C (Alix antibody, 1/500, ab117600; anti-HSP70 antibody,1/500, ab181606; anti-CD63 antibody, 1/500, ab134045; anti-CD81 antibody, 1/500, ab155760; TSG101 antibody, 1/500, ab125011; Calnexin antibody, 1/1000, ab22595, Abcam). The membranes were rinsed and incubated with secondary antibodies for 1 h with anti-rabbit, peroxidase-conjugated IgG secondary antibodies (#711-035-152, Jackson ImmunoResearch) diluted to 1/10,000 in TBST (Tris-buffered saline, 0.1% Tween 20). Protein-antibody complexes were visualized by chemiluminescence with the SuperSignal West Pico Chemiluminescent Substrates (Pierce) using a ChemiDoc MP gel imaging system (Bio-Rad). Densitometry analysis of the protein expression was normalized to expression of the loading controls glyceraldehyde-3-phosphate dehydrogenase (GAPDH, 1/10,000, ab8245, Abcam) or tubulin (1/20,000, sc-32293, Santa Cruz Biotechnology) and performed using ImageJ. The particle size of the exosomes was measured with transmission electron microscopy (Hitachi HT7800) and NanoSight analysis (NanoSight NS300).

2.6. Western blot analysis and immunofluorescence of iPSCs

Equal amounts of protein (30 μg) in SDS-PAGE sample buffer were sonicated and subjected to electrophoresis on 12% SDS-polyacrylamide gels. After transfer to PVDF membranes, proteins were incubated with primary antibodies (OCT4, 1/1000, ab19857; SOX2, 1/1000, ab97959; NANOG, 1/1000, ab21624; SOX17, 1/1000, ab155402; PAX6, 1/1000, ab5790; Brachyury, 1/1000, ab20680, Abcam). The membranes were prepared and analyzed with secondary antibodies as described above. Densitometry analysis of the protein expression was normalized to expression of the loading controls GAPDH (1/10,000, ab8245, Abcam) or tubulin (1/20,000, sc-32293, Santa Cruz Biotechnology) and performed using ImageJ. A minimum of three experimental repeats were used to perform the statistical analyses.

To perform immunostaining, samples were washed in PBST and blocked with 2% bovine serum albumin (BSA) for 30 min at room temperature. Samples were then incubated overnight at 4 °C with primary antibodies against OCT4 (1/1000), YAP (1/200, #14074, Cell Signaling), phospho-YAP (1/200, ab172374, Abcam) for iPSCs or cleaved Caspase-3 (1/400, D175, Cell Signaling) for the recipient cells treated with iPSC-derived exosomes. Samples were subsequently stained with fluorescently labeled secondary antibodies with AF 546 goat anti-rabbit secondary antibodies (1/500, Life Technologies) overnight at 4 °C. Addition of phalloidin-633 (actin stain, 1/250), and 4,6-diamidino-2-phenylindole (DAPI) (nuclear stain, January 2000 dilution in PBST, 2 h) were performed on the next day. Samples were washed and mounted for visualization on a Leica confocal microscope (DMI4000 B). The mean fluorescence intensity (MFI) was determined as the mean of the regions of interest (ROIs) in ImageJ software. MFI of target proteins was normalized to MFI of DAPI as an internal control to account for sample to sample variations. A minimum of three experimental repeats were used to calculate the averages and to perform the statistical analyses.

2.7. Reverse transcription PCR (RT-PCR)

Total RNA was isolated using a TRIzol® Reagent (Ambion) and phenol-chloroform extraction with a Phase Lock Gel (5 PRIME) according to the manufacturer's protocol. The amount of the total RNA from each sample was quantified using a Nanodrop1000 spectrophotometer (Thermo Fisher Scientific). Reverse transcription of isolated RNA was then performed using a T100 Thermal Cycler (Bio-Rad) according to the manufacturer's protocol. Using serial dilutions of cDNA, qPCR was performed for several stem cell lineage genes including SOX16 (Endoderm), PAX6 (Ectoderm), and HAND1 (Mesoderm). All the expression values were normalized to the GAPDH housekeeping gene. See Supplemental Table S1 for primer sequences.

2.8. Validation of exosome uptake

Mouse NIH 3T3 cells, human umbilical vein endothelial cells (HUVECs) and Madin-Darby Canine Kidney (MDCK) cells were cultured and maintained following the supplier's protocols. A cell seeding concentration of 4000 cells/cm^2 was used for all analyses. Exosomes were labeled with PKH-67 (Sigma-Aldrich) to determine cellular uptake. In accordance with the manufacturer's protocol, exosomes diluted in 1 ml Diluent C and 4 μl PKH26 dye diluted in 1 ml Diluent C were incubated together. After 4 min, 2 ml 0.5% BSA in DPBS was added to bind excess dye. The labeled exosomes were washed in DPBS at 100,000 g for 1 h. Afterward, the labeled exosomes (5 μg/ml) were incubated with cells for 24 h. After incubation, cells were washed twice with DPBS, fixed in 4% paraformaldehyde for 10 min, and washed again. Images were captured with a DMI4000 B confocal microscope (Leica).

2.9. Cell proliferation assay

To measure cell proliferation, the lysed cell samples (5 μl) were aliquoted into black 384-well plates, mixed with 20 μl of Tris-EDTA (TE) buffer, and incubated with 30 μl of Quant-iT PicoGreen dsDNA assay reagent (Life Technologies) working solution, diluted in 1× TE buffer (1:200) according to the manufacturer's instructions, incubated for 5 min protected from light at room temperature. Fluorescence signal (excitation 485 nm, emission 520 nm) was detected using a fluorescence plate reader (Multimode Microplate Reader, Model M2, Molecular Dynamics).

2.10. Mouse NIH 3T3 cell serum starvation test

NIH 3T3 fibroblast cells (ATCC) were cultured in high glucose Dulbecco's modified Eagle's medium (DMEM) (Gibco, USA) supplemented with 10% Fetal Bovine Serum (FBS), 100 U/ml penicillin, and 100 mg/ml streptomycin and maintained in a humidified atmosphere and 5% CO2 at 37 °C. Medium was renewed every 2–3 days until 3T3 fibroblasts reached 80–90% confluence. At this point, cell passage was conducted and culture medium without FBS was used to induce cell starvation, and cells were treated with iPSC-derived exosomes (5 μg/ml or 0.5 μg/ml), DPBS only as negative control, or standard medium containing FBS (10%) as a positive control (never exposed to serum starvation). After 48 h, cell viability and spreading area were measured using PicoGreen and CellTracker™ Red CMTPX (C34552, Invitrogen), respectively. Briefly, cell spreading area were detected using automatic edge detection (ImageJ) with 100× magnification based on at least 10 full images in each group in three independent experiments (λ_{ex} = 580 nm, λ_{em} = 650 nm for TRITC/CellTracker™ visualization).

2.11. HUVEC hypoxia test

HUVECs (PromoCell) were maintained in HUVEC growth medium (EGM-2 Bullet Kit, Lonza). Fresh medium was changed every three days. Cells were washed twice with DPBS and detached with 0.25% trypsin and EDTA (Sigma-Aldrich) for passage. Passages between 3 and 5 were used in our experiments. Once HUVEC reached about 80% confluence, cultures were serum-starved thereafter and exposed to a hypoxic environment of 0% O_2 at 37 °C. Following this, HUVECs were also treated with either iPSC-derived exosomes (5 μg/ml or 0.5 μg/ml), or DPBS as negative control. Standard maintenance medium with 95% air and 5% CO_2 was a positive control. After a further 48 h of exosome treatment, HUVEC morphology was imaged by phase contrast microscopy (Zeiss, Axiovert 200 M), and DNA content was quantified using PicoGreen assay as described above.

2.12. MDCK cell hyperosmolarity test

Type II MDCK cells were grown to subconfluence, rinsed twice with DMEM, and switched to hypertonic medium without FBS to induce hyperosmolarity stress. Hypertonic medium was made by addition of NaCl to a final total concentration of 600 mOsm/L. After initiating hyperosmolarity stress, cells were treated with iPSC-derived exosomes (5 μg/ml or 0.5 μg/ml), DPBS only as negative control, or standard DMEM plus 10% FBS as a positive control. After 48 h, LIVE/DEAD viability/cytotoxicity assay was performed according to the manufacturer's protocol (Molecular Probes). Labeled cells were imaged using a confocal microscope (Leica), and at least three fields of view were imaged for each sample.

2.13. Caspase-3/7 assay

For detection of apoptotic cells, Caspase-3/7 assay was performed using an Apo-ONE™ Homogeneous Caspase-3/7 assay kit (Promega) according to the manufacturer's recommendations. After undergoing the stress of serum starvation, hypoxia, or hyperosmolarity for 24 h, cells were collected and then stored at 4 °C in lysis buffer (pH 7.4, 150 mM NaCl, 20 mM Tris HCl, 0.5% Triton X-100) prior to analysis.

2.14. RNA purification from exosomes

Exosome RNA was isolated using a procedure described in the exoEasy Handbook (QIAGEN). Briefly, purified exosomes were bound on the exoEasy membrane affinity column, the vesicles were lysed by adding QIAzol to the spin column and further collected by centrifugation (exoRNeasy, QIAGEN). Following chloroform extraction, samples were thoroughly mixed and centrifuged to separate organic and aqueous phases. The aqueous phase was recovered and mixed with ethanol. The sample-ethanol mixture was added to a RNeasy MinElute spin column and centrifuged. The column was washed once with buffer RWT and then twice with buffer RPE followed by elution of RNA in water. The RNA concentration, purity, and integrity were assessed using the RNA Nano 6000 Assay Kit of the Agilent Bioanalyzer 2100 System (Agilent Technologies, CA, USA).

2.15. Small RNA library construction and sequencing

Prior to sequencing experiments, RNA concentration, purity, and integrity were assessed using the RNA Nano 6000 Assay Kit of the Agilent Bioanalyzer 2100 System (Agilent Technologies, CA, USA). Illumina sequencing libraries were prepared using the NEXTflex™ small RNA-seq kit v3 Guide (Bioo Scientific, 5132–05), according to the manufacturer's instructions. For each library, 60 ng of purified Exosome RNA were ligated to 3′ and 5′ adaptors and then reverse transcribed to cDNA using adaptor-specific primers. After purification and PCR amplification using universal and specific barcode primers, the miRNA library was resolved and recovered from the 6% TBE-PAGE gel based on the corresponding size for miRNA distribution. The yield and size distribution of the small RNA libraries were assessed using the Agilent 2100 Bioanalyzer instrument with the High-Sensitivity DNA Assay (Agilent Technologies). Equal concentration of each library was sequenced on a NextSeq 500 (Illumina) platform.

2.16. Sequencing data analysis and bioinformatics analysis

Upon completion, sequencing data were assessed for quality and trimmed of the primer-adaptor sequences by the Partek® Flow® Genomic Analysis Software (Partek), followed by alignment to the human reference genome (hg38) (by bowtie 2). After annotation of known miRNA based on miRBase, the number of reads for each miRNA was normalized to reads per million (RPM) and quantified across all samples. The statistical package of Partek® Flow® Genomic Analysis Software was used to yield differential expression, volcano plot, and hierarchical clustering analyses. miRNA target prediction was compiled by the microRNA Target Filter analysis module of Ingenuity Pathway Analysis (IPA, QIAGEN), while target pathway annotations were done by the Core Analysis of IPA.

2.17. Statistics and data analysis

All experiments were performed at least three times. All data are presented as mean ± standard deviation. ANOVA with *post hoc* Bonferroni test is utilized to identify statistically significant differences using SPSS software (version 17.0 for Windows; SPSS Inc, Chicago, Illinois, USA). Differences are considered statistically significant when $p < 0.05$. For Figs. 7–10, due to the large number of statistically significant data points, the statistical significance on the graphs are depicted relative to the control condition of no exosome treatment only. For completeness, all other p value results are shown in Supplemental Table S2.

3. Results and discussion

3.1. Human iPSC proliferation and morphology on engineered substrates

Recombinant ELPs containing either the RGD or RDG peptide sequences were expressed in *Escherichia coli* and confirmed by Western blot as described above (Fig. S1A,B). ELP was adsorbed onto tissue culture polystyrene by incubation overnight at 4 °C, while Matrigel substrates were prepared by incubation for 30 min at 37 °C. Similar to previous reports, this protocol consistently resulted in 2.0–4.0 μg/cm^2 of ELP coating for both the RGD and RDG variants across days 1–3 of culture and 5.0–8.0 μg/cm^2 of Matrigel (Fig. S1C). Cultures were plated on freshly prepared substrates for all experiments to standardize the procedure. The morphology of human iPSCs from two different cell lines (iPSC SCVI480 and iPSC 511.3) (Fig. 1A and B) consistently demonstrated greater cell spreading on Matrigel, slightly less spreading on ELP substrates containing the RGD peptide (*i.e.* RGD-ELP), and dramatically less spreading on ELP substrates with the scrambled RDG peptide (Fig. 1C). RDG-elastin contains a scrambled amino acid sequence in which the aspartate and glycine residues in the minimally active tripeptide were reversed, but was otherwise identical. This change in amino acid sequence was previously reported to prevent integrin-mediated cell spreading in ELP materials [48,49]. Colonies on the non-integrin-engaging, RDG substrate (*i.e.* RDG-ELP) were more compact and rounded, while those grown on Matrigel and RGD-ELP substrates had a flatter appearance on day 3. Together, these results suggest that the RGD-ELP and Matrigel substrates result in a more spread morphology due to interactions with integrins known to be present on iPSCs. Interestingly, the DNA content of both stem cell lines was statistically similar at day 3 across all three culture substrates (Fig. 1D), suggesting that proliferation capacity was not affected by the observed changes in morphology.

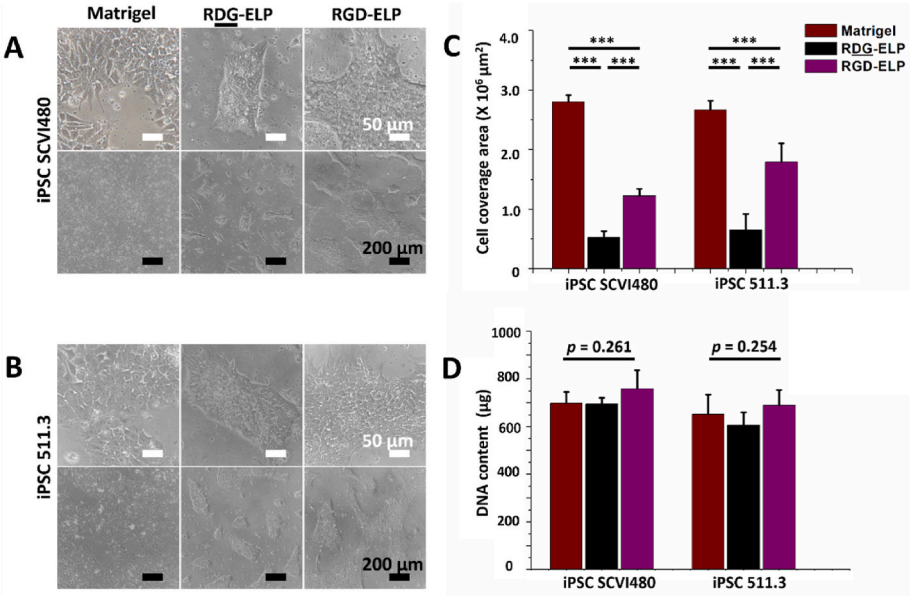

Fig. 1. Two iPSC cell-lines cultured on Matrigel, RDG-ELP, and RGD-ELP substrates are presented. (A and B) The cell morphology as determined by phase contrast microscopy, (C) cell coverage area, and (D) DNA content of two iPSCs cell lines (iPSC SCVI480 and iPSC 511.3) grown on different coatings at day 3. All data presented as mean±standard deviation; ***$p < 0.001$.

3.2. iPSC phenotype is influenced by engineered ELP substrates

Before confirming that iPSCs were capable of producing exosomes on the engineered ELP substrates, we sought to evaluate any potential changes in iPSC phenotype that might arise in response to RGD-ELP *vs.* RDG-ELP. The expression of the stemness markers OCT4, SOX2, and NANOG were examined by Western blot analysis. Cells grown on RGD-ELP had significantly lower levels of OCT4 expression (normalized to the loading control GAPDH) compared to cells grown on RDG-ELP or Matrigel (all $p < 0.001$, Fig. 2A and B). Similarly, the stemness markers SOX2 and NANOG were expressed at lower levels by cells grown on RGD-ELP than on RDG-ELP or Matrigel (all $p < 0.001$; normalized to the loading control Tubulin to avoid molecular weight overlap between SOX2/NANOG and GAPDH, Fig. 2A, B and Fig. S2, respectively). These results were further confirmed through the MFI of immunostaining for OCT4 for both cell lines iPSC SCVI480 and 511.3 (Fig. 2C–F and Fig. S3). Quantification showed that OCT4 expression (normalized to a DAPI nuclear stain) was significantly decreased for iPSCs cultured on RGD-ELP compared to cells on RDG-ELP or Matrigel (all $p < 0.001$, Fig. 2D, F and Fig. S3B). Previous reports have used Matrigel at a diluted concentration, similar to that used here, to form coatings that maintain the pluripotent, proliferative phenotype of stem cells [50,51]. When used undiluted, Matrigel is reported to promote stem cell differentiation, suggesting that an increased density of cell-adhesive ligands may initiate differentiation [52–54]. Thus, we hypothesize that perhaps the high concentration of cell-adhesive RGD ligands within the RGD-ELP substrate may be responsible for the onset of spontaneous differentiation compared to cells on diluted Matrigel or the RDG-ELP substrate.

We also examined how these three coating substrates affected the gene expression levels of several markers of stemness (OCT4 and

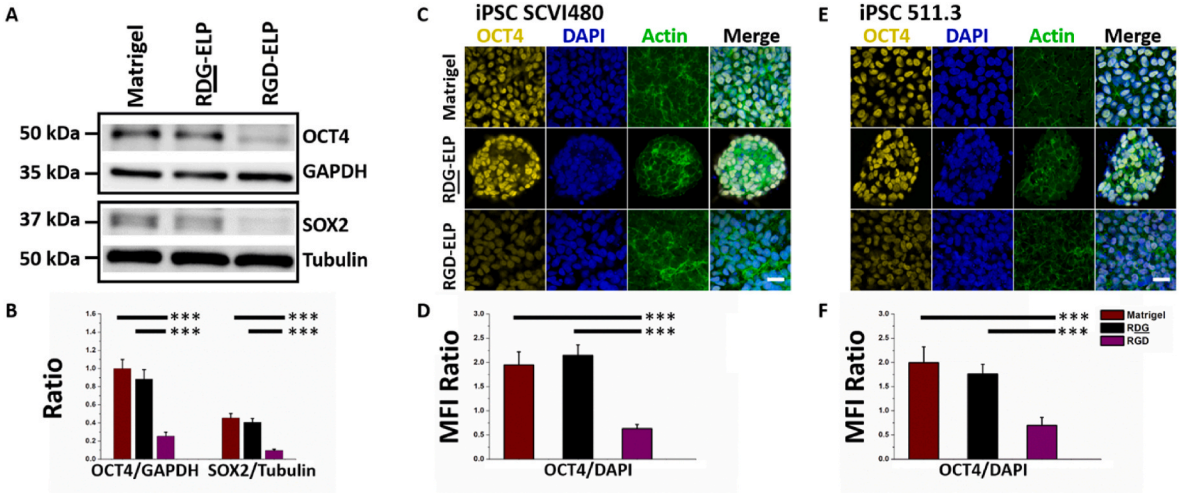

Fig. 2. Protein expression of stemness markers on ELP substrates. (A) Western blot of OCT4 and SOX2 for iPSCs grown on Matrigel, RDG-ELP, or RGD-ELP. (B) Western blot quantification of OCT4/GAPDH and SOX2/tubulin protein levels. (C–E) Immunocytochemistry for OCT4 (yellow), nuclei (DAPI stain, blue), and actin (phalloidin stain, green) of iPSC SCVI480 (C, D) and iPSC 511.3 (E, F) cultured on different substrates. Scale bar = 25 μm. (E, F) Quantification of OCT4 immunocytochemistry is reported relative to DAPI using mean fluorescence intensity (MFI) for iPSC SCVI480 (E) and iPSC 511.3 (F). All data presented as mean±standard deviation; ***$p < 0.001$. (For interpretation of the references to colour in this figure legend, the reader is referred to the Web version of this article.)

NANOG) and differentiation (SOX17, PAX6, and HAND1 as markers of endoderm, ectoderm, and mesoderm differentiation, respectively, Fig. 3 and Fig. S4). Cells grown on all substrates expressed high levels of mRNA for the stemness markers OCT4 and NANOG, with no statistically significant differences. Thus, while protein-level data suggest subtle yet statistically significant changes in cell stemness on different substrates (Fig. 2 and Fig. S3), all cultures could still be classified as pluripotent stem cells through mRNA-level analysis (Fig. 3A, B and Fig. S4). These data are consistent with the use of an E8 culture medium, which was formulated to maintain pluripotency [55].

The differences between levels of protein translation (Fig. 2, S2, and S3) and mRNA transcription (Fig. 3 and S4) for the stemness markers could be due to the complexity of post-transcriptional processes of gene expression regulation, especially during dynamic transitions. The association between the concentration of coding transcripts and protein levels is dependent on several factors including the local availability of resources for protein expression and post-transcriptional processes [56]. Large deviations from the ideal 1:1 correlation between mRNA and protein levels are commonly observed during highly dynamic cellular phases, including differentiation and stress responses [57].

Interestingly, although all markers of differentiation (SOX17, PAX6, and HAND1) were expressed several orders of magnitude lower than the stemness markers (OCT4 and NANOG), there were statistically significant changes between the different substrates. Cells grown on RGD-ELP had significantly higher mRNA levels for all three differentiation markers compared to cells grown on RDG-ELP or Matrigel ($p < 0.001$ for all comparisons, Fig. 3C–E and Fig. S4C-E). Significantly increased SOX17, PAX6, and Brachyury protein expression, markers of endoderm, ectoderm, and mesoderm differentiation, respectively [58,59], on RGD-ELP substrates was also confirmed through Western blot ($p < 0.01$ compared to RDG-ELP or Matrigel, Fig. S5). Taken together, these data reinforce the notion that subtle phenotypic differences exist when iPSCs are cultured on RDG-ELP *vs.* RGD-ELP substrates that suppress spontaneous differentiation.

Matrix adhesion-dependent cell proliferation and differentiation is associated with the Hippo signaling cascade, which includes the action of Yes-associated protein (YAP) [60,61]. YAP activity is known to regulate proliferation and differentiation in several stem and progenitor cell types [62,63]. YAP activity can be regulated through the overall level of protein expression [64,65] and/or by changes in phosphorylation that result in subcellular localization [66,67]. Thus, we were interested to see if YAP protein levels or YAP subcellular localization were altered for iPSCs grown on these different ELP substrates, including RDG-ELP, RGD-ELP, or non-ELP-coated controls (tissue culture plastic only). Through immunocytochemistry staining, we observed that YAP protein was primarily found in the cytoplasm for iPSCs cultured on all three substrates and was not localized to their nuclei (Fig. 4 and Fig. S6). Interestingly, quantification of total YAP immunofluorescence and Western blotting found significantly lower levels of YAP expression for cells grown on RGD-ELP compared to RDG-ELP or non-coated controls (Fig. 4C and Fig. S6C, $p < 0.001$). Across all substrates, YAP was observed to be located in the cytosol rather than the cell nuclei (Fig. 4B and Fig. S6B). The ratio of phosphorylated YAP to total YAP was not significantly different (ANOVA, $p = 0.513$), which means the activated form of phosphorylated YAP in the RGD-ELP group had substantially lower levels than the other two groups (Fig. 4D). Interestingly, expression of the integrin sub-unit β1 (ITGβ1) was significantly increased on the RGD-ELP culture group compared to RDG-ELP and control cultures ($p = 0.003$ and $p < 0.001$, respectively) (Fig. 4E). This integrin sub-unit is well known as a receptor for the RGD tripeptide present in the RGD-ELP substrate [40,68]. These data suggest there may be a feedback mechanism on the RGD-ELP substrate, whereby integrin engagement with the RGD peptide leads to further increased expression of the integrin sub-unit β1.

3.3. Collection and verification of iPSC-derived exosomes

Exosomes were collected from human iPSC-conditioned supernatants of cultures grown on Matrigel or ELP substrates containing the RGD or RDG peptides. Exosomes were purified by PEG precipitation and ultra-centrifugation [47]. The procedure for PEG precipitation is simple, fast, and scalable; it does not deform exosomes, and provides a low-cost procedure for isolation [69,70]. The main drawback of PEG precipitation is possible contamination with other protein complexes [71]; however, impurities can be limited by subsequent centrifugation [72]. NanoSight particle-tracking analysis and transmission electron microscopy confirmed exosome production (Fig. 5A and B). All exosome samples were of similar size and within the typical size range reported

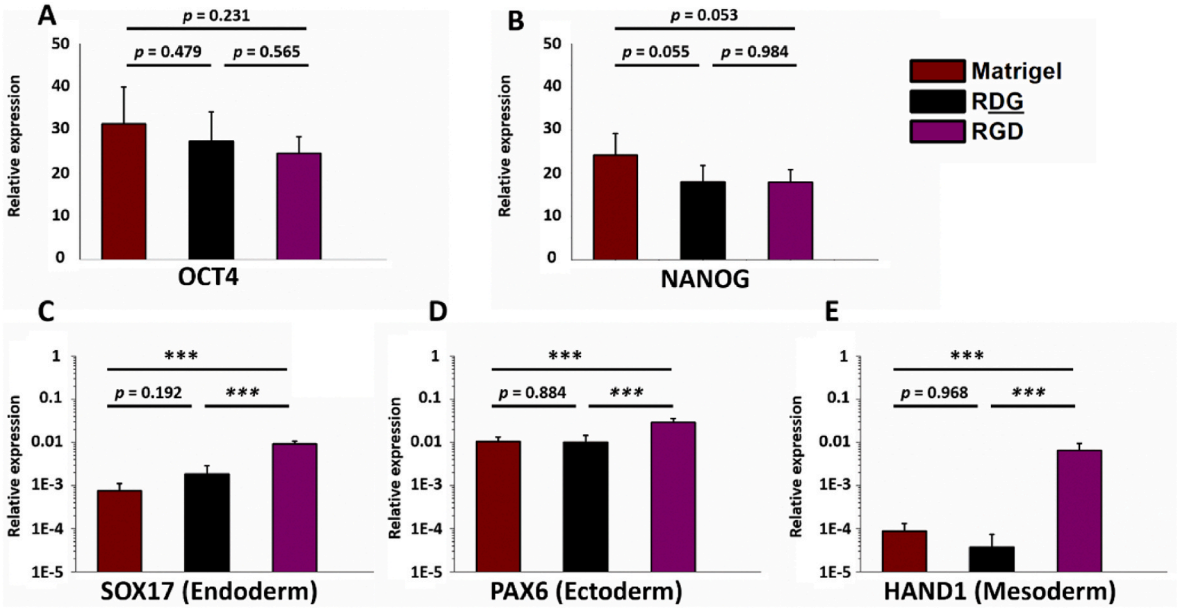

Fig. 3. QRT-PCR analysis of mRNA expression for iPSCs (SCVI480) grown on various substrates. Quantitative analysis of stemness markers (A) OCT4 and (B) NANOG and lineage markers of (C) endoderm (SOX17), (D) ectoderm (PAX6), and (E) mesoderm (HAND1) for cells grown on different substrates in E8 culture medium for 3 days. Relative expression levels were normalized against GAPDH. ***$p < 0.001$.

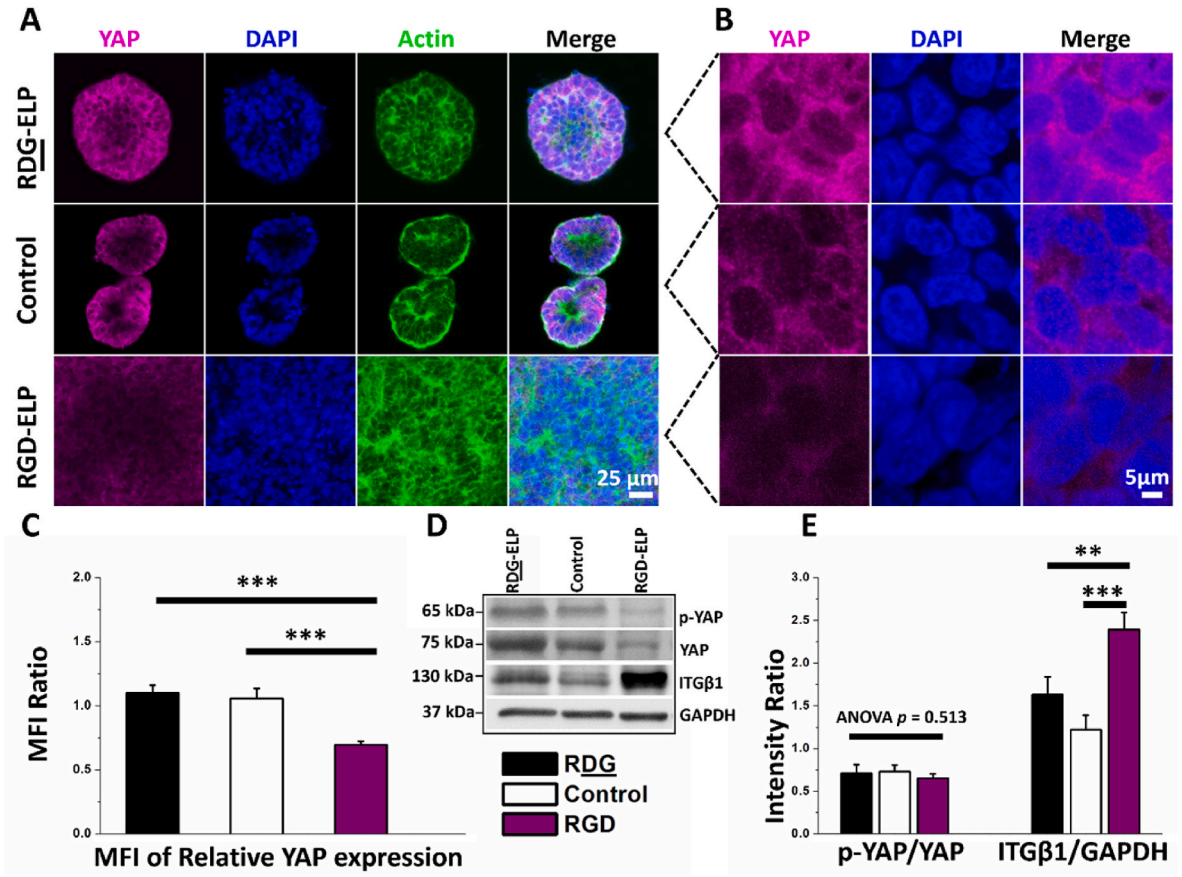

Fig. 4. YAP expression and quantification in iPSCs on various substrates. (A–B) Immunofluorescence of YAP in iPSCs (SCVI480) grown for three days on RDG-ELP, non-coated, or RGD-ELP plates. (A) Scale bar = 25 μm. (B) Scale bar = 5 μm. The accumulation of YAP signal was mainly observed in the cytoplasm for all substrates. (C) MFI quantification of total YAP immunofluorescence suggests lower YAP expression for iPSCs cultured on RGD-ELP substrates. (D and E) Western blot analysis (D) and quantification (E) for phosphorylated YAP (p-YAP), total YAP, and integrin sub-unit β1 (ITGβ1). ***$p < 0.001$; **$p < 0.01$.

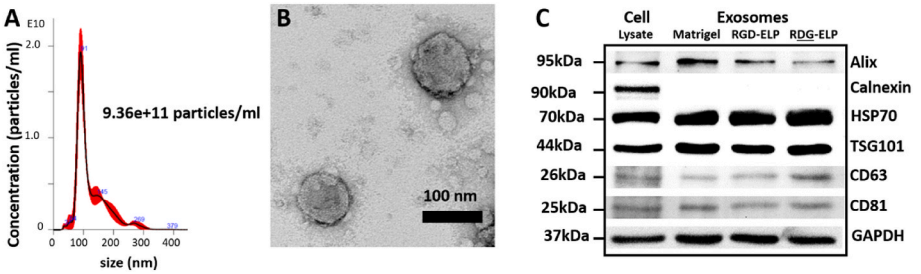

Fig. 5. Characterization of iPSC-derived exosomes produced on three different substrates: RDG-ELP, RGD-ELP, or Matrigel. (A) The graph represents size distribution of nanoparticles collected from cultures on Matrigel, as characterized by NanoSight particle-tracking analysis. (B) Transmission electron microscopy of samples from Matrigel depicts multiple cup-shaped, shrunken vesicles (C) Western blot for positive (Alix, HSP70, TSG101, CD63, CD81) and negative (calnexin) exosomal markers for the three substrate groups and a cell lysate control.

for exosomes (30–150 nm in diameter), with mean diameters of 81.3 ± 5.0, 88.0 ± 4.3 nm, and 82.2 ± 4.7 nm for those produced on Matrigel (Fig. 5A and B), RDG-ELP (Fig. S7A), and RGD-ELP (Fig. S7B), respectively [73,74]. Western blot analysis demonstrated that exosomes produced by cells on all three substrates were positive for proteins commonly used as exosome markers: Alix, heat shock protein (HSP70), CD63, CD81, and tumor susceptibility gene 101 protein (TSG101), which is part of the endosomal sorting complex required for transport [75], and negative for calnexin, consistent with previous literature [76,77]. As expected, all proteins, including calnexin, were detected from the full cell lysate as a positive control. Quantification and normalization to GAPDH as a housekeeping gene confirmed that the loading protein content was similar across all three substrates (Fig. 5C).

3.4. *In vitro* analysis of exosome potency

The ability of the iPSC-produced exosomes to be taken up by other cells was confirmed using confocal microscopy. Three types of cells (mouse fibroblasts (NIH 3T3 line), human umbilical vein endothelial cells (HUVEC), and Madin-Darby canine kidney (MDCK) cells) were treated with iPSC-derived exosomes labeled using PKH-67 (green). After 2 h of treatment, exosomes were observed to be localized within the treated cells (Fig. 6 and Fig. S8).

After binding to cells, exosome contents are internalized by recipient cells, which can result in the transfer of bioactive molecules that exert functional effects including pro-survival activity [78,79]. To characterize potential differences in pro-survival potency for exosomes produced on different substrates, we tested these iPSC-derived exosomes in three different cell survival challenge assays. First, we tested exosome potency on murine fibroblasts in a serum starvation challenge. When

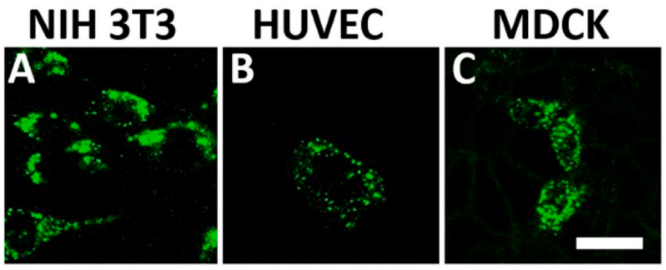

Fig. 6. Exosomes derived from iPSCs (SCVI480) localize with multiple cell types. (A–C) Representative fluorescent micrographs of PKH67 labeled exosomes (green) with mouse NIH 3T3 fibroblasts, HUVEC, and MDCK cells after treatment *in vitro* for 2 h (Scale bar is 25 μm). (For interpretation of the references to colour in this figure legend, the reader is referred to the Web version of this article.)

deprived of serum rich in essential growth factors [80], NIH 3T3 cells arrest in a nondividing, quiescent state, which eventually leads to starvation-induced cell death [81]. While healthy fibroblasts typically exhibit a spindle-like, elongated morphology, after 48 h of serum starvation NIH 3T3 fibroblasts exhibited a rounded cell morphology (Fig. 7 and Fig. S9). Treatment with exosomes (5 μg/ml) produced by iPSCs cultured on RDG-ELP or Matrigel substrates significantly improved serum-starved fibroblast spreading (as observed by fluorescent CellTracker, $p < 0.001$). In contrast, treatment with exosomes produced by iPSCs cultured on RGD-ELP did not statistically improve serum-starved fibroblast morphology ($p = 0.326$).

We also quantified total levels of fibroblast DNA as a higher throughput assay of serum starvation effects using different iPSC cell line-derived exosomes including SCVI480, 511.3, and IBMS-iPSC-001-02 (Fig. S10). Even at this relatively early timepoint of 48 h, statistically significant differences in DNA were observed for fibroblasts with and without 5 μg/ml exosome treatment, although differences between exosomes from iPSCs grown on different substrates were not as apparent. Exosomes from all different iPSC cell lines were found to be protective, and the exosome effect appeared to be dose-dependent, as a dosage of 0.5 μg/ml produced fewer protective effects than a dosage of 5 μg/ml (Fig. S10B).

As a second test of exosome potency, we explored the effects of hypoxia (0% O_2) on HUVECs. After 48 h of hypoxia, DNA content was about 50% of that of cells grown in normoxia, suggesting a decrease in cell proliferation and an increase in cell death, which was confirmed by bright field microscopy (Fig. 8A). Exosomes are known to be capable of improving endothelial cell proliferation and survival [82,83]. HUVEC were treated with either 5 or 0.5 μg/ml of exosomes produced from three iPSC cell lines grown on RDG-ELP, RGD-ELP, or Matrigel (Fig. 8 and Fig. S11). Similar to the trends observed for the fibroblast serum starvation assay, the greatest amount of HUVEC rescue was observed upon treatment with 5 μg/ml of exosomes from RDG-ELP, which had DNA levels of 94 ± 9% of normoxia controls (Fig. 8E). While exosome treatment at the lower dosage of 0.5 μg/ml was able to statistically improve HUVEC DNA levels for exomes prepared on RDG-ELP or Matrigel substrates ($p < 0.05$ for both), exosomes prepared from RGD-ELP substrates approached significance ($p = 0.058$) for the SCVI480 cell line (Fig. 8E).

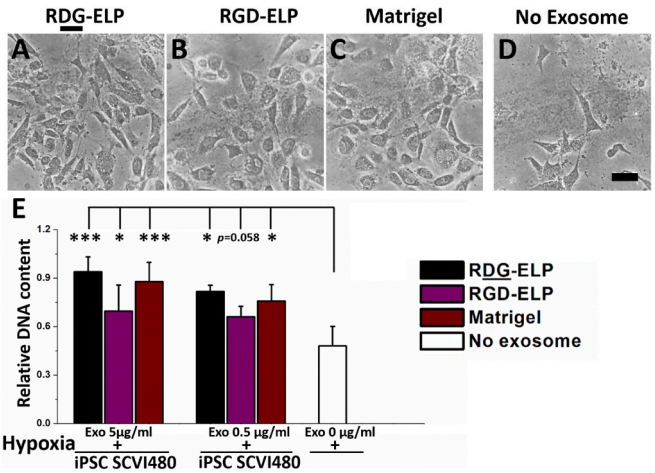

Fig. 8. HUVEC hypoxia challenge. (A–D) Representative phase contrast micrographs of HUVEC following 48 h hypoxia with or without iPSC-derived (SCVI480) exosome treatment. Less cells are noted in images without exosome treatment. (E) PicoGreen assay to quantify HUVEC DNA upon treatment with 5 μg/ml or 0.5 μg/ml of exosomes prepared from iPSCs cultured on RDG-ELP, RGD-ELP, or Matrigel substrates. Data presented relative to a normoxic HUVEC control. $^{*}p < 0.05$, $^{***}p < 0.001$. Scale bar = 10 μm.

As a third test of exosome potency, MDCK cells were subjected to hyperosmolarity. Hyperosmolarity, or hypertonicity, is known to induce cell death and apoptosis [84,85]. As a more sensitive read-out of cellular health, we employed a commercial Live/Dead assay to fluorescently label cells with compromised cell membrane. After 48 h in 600 mOsm/L medium conditions (Fig. 9 and Fig. S12), consistent with the exosome potency trends observed in the previous two cellular challenge assays, exosomes produced on RDG-ELP or Matrigel substrates resulted in significant improvement in Live/Dead ratios ($p < 0.001$ for both substrates for exosomes produced by SCVI480 and IBMS-iPSC-001-02, Fig. 9E and S12E). Exosomes produced on RGD-ELP substrates were not statistically effective ($p = 0.432$, Fig. 9E for SCVI480, and $p = 0.398$, Fig. S12E for IBMS-iPSC-001-02). MDCKs exhibited only a mild decrease in total DNA

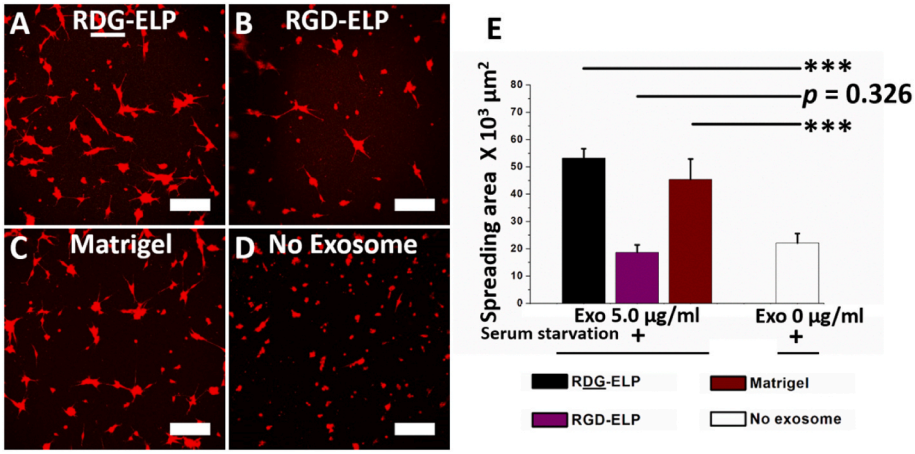

Fig. 7. NIH 3T3 fibroblast serum starvation challenge. (A–D) Representative micrographs of NIH 3T3 fibroblasts labeled with CellTracker (red) to visualize cell morphology upon serum starvation for 48 h. (E) Quantification of serum-starved fibroblast spread area with or without treatment of exosomes (5 μg/ml) produced by iPSCs (SCVI480) grown on RDG-ELP, RGD-ELP, or Matrigel substrates. Scale bar = 200 μm. (For interpretation of the references to colour in this figure legend, the reader is referred to the Web version of this article.)

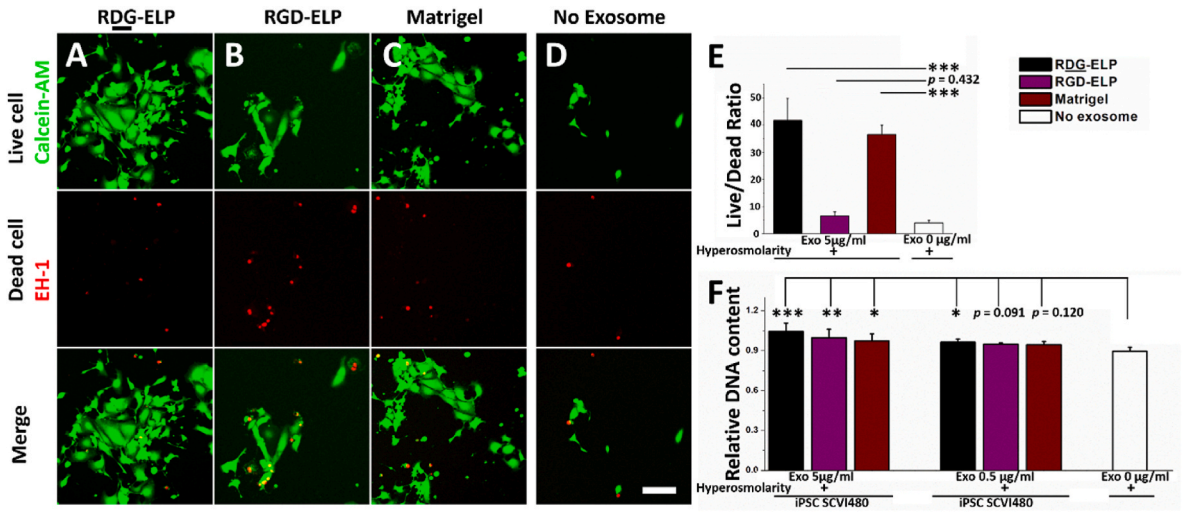

Fig. 9. MDCK hyperosmolarity challenge. (A–D) Representative Live/Dead (green/red) confocal images and (E) quantification of MDCKs exposed to 600 mOsm/L for 48 h with or without treatment of 5 μg/ml exosomes produced on various substrates from SCVI480 iPSCs. (F) PicoGreen DNA quantification of MDCK cells exposed to hyperosmolarity with or without treatment of 5 μg/ml or 0.5 μg/ml exosomes produced on RGD-ELP, RDG-ELP, or Matrigel substrates. $^{*}p < 0.05$, $^{**}p < 0.01$, $^{***}p < 0.001$. Scale bar = 100 μm. (EH-1, Ethidium homodimer-1). (For interpretation of the references to colour in this figure legend, the reader is referred to the Web version of this article.)

content (Fig. 9F), as measured by PicoGreen assay (90 ± 3% compared to normal medium conditions) using the exosomes that were produced from iPSC SCVI480. Nonetheless, statistically significant improvements in total DNA were observed upon treatment with 5 or 0.5 μg/ml of exosomes produced from SCVI480 on RDG-ELP substrates ($p < 0.001$ and $p < 0.05$, respectively) as well as with exosomes produced by the other two tested iPSC cell lines (Fig. S13).

Apoptosis is a common mechanism of cell death in response to serum starvation, hypoxia, and hyperosmolarity. Stem cell-derived exosomes have been reported to play an inhibitory role in cell apoptosis both *in vitro* and *in vivo* [86,87]. Thus, we sought to directly examine if our iPSC-derived exosomes were altering apoptotic pathways during the three challenge assays described above. By immunocytochemistry, survival-challenged cells treated with 5 μg/ml of RDG-ELP-prepared exosomes had less appearance of caspase-3 than the cells exposed to the survival challenge alone (Fig. 10A, B, C). Similar observations were made for serum-starved fibroblasts, hypoxia-challenged HUVEC, and hypertonicity-challenged MDCK, all of which were challenged for 24 h prior to assessment. Longer challenge timepoints were not used to prevent loss of cells and hence loss of statistical sensitivity. To quantify caspase 3/7 activity, the Apo-ONE Homogeneous Caspase 3/7 assay was used. For all three challenge assays, 24 h of exposure to the survival challenge significantly increased caspase 3/7 activity ($p < 0.001$ for all three assays, Fig. 10D, E, F and Fig. S14). For all three cell challenges, standard medium was used as a positive control (never exposed to the cell challenges) and similar trends were observed, with exosomes produced on RDG-ELP or on Matrigel substrates all resulting in a significant reduction in caspase 3/7 activity (Fig. 10D, E, F and Fig. S14). In contrast, exosomes produced on RGD-ELP substrates had a less significant effect on caspase 3/7.

Exosomes can transmit molecular cargo between cells, with accumulating evidence suggesting that exosomal microRNAs play a leading mechanistic role in the therapeutic effects of exosomes. Hierarchical clustering (Euclidean distance) of the differentially expressed miRNAs of exosomes from iPSCs cultured on RDG-ELP, RGD-ELP, or Matrigel were illustrated in a heatmap representation (Fig. 11A). Exosomal miRNAs from iPSCs grown on RDG-ELP participated in several molecular signaling pathways, including p53 most prominently and several apoptosis signaling pathways (Fig. 11B, Fig. S15, Supplemental Table S3). Specifically, we identified five iPSC-derived exosomal miRNAs that were differentially expressed by cells on the RDG-ELP substrates and are known to be involved in the regulation of apoptotic pathways (Supplemental Table S3), suggesting that these miRNAs may be at least partially responsible for the observed effects on *in vitro* cultures. Interestingly, the level of miR-378a-3p, which targets CASP9 and is known to inhibit apoptosis [88], was found at significantly higher levels in exosomes derived from iPSCs cultured on RDG-ELP compared to RGD-ELP (counts per million: RDG-ELP 8754 ± 614 vs. RGD-ELP 2689 ± 215, $p = 0.032$). These data are consistent with our observations of lower apoptotic activation, as measured by caspase3/7 activity, for *in vitro* cultures that were treated with RDG-ELP-produced exosomes compared to exosomes produced on RGD-ELP substrates (Fig. 10D–F and Fig. S14). Taken together, these data strongly suggest that hiPSCs cultured on less adherent, protein-engineered substrates express higher levels of miRNAs that can downregulate apoptotic genes and subsequently induce an anti-apoptotic and pro-survival effect on challenged *in vitro* cell cultures. Future mechanistic work will be required to identify the most causative miRNA for altered apoptotic regulation in this system, as well as to test for other potential effects such as alteration of cell proliferation.

In summary, the three challenge assays described above confirm our original hypothesis, that iPSC-derived exosome potency can be altered by the underlying culture substrate used when producing exosomes. In general, all three challenge assays had similar trends in exosome potency, with iPSCs cultured on the strongly cell-adhesive RGD-ELP substrates producing the least potent exosomes (Figs. 7–10). In contrast, iPSCs grown on RDG-ELP substrates produced exosomes with similar levels of potency as iPSCs grown on diluted Matrigel (Figs. 7–10). These data further demonstrate that the potency of these iPSC-derived exosomes have potential effects across a range of mammalian cell types exposed to a variety of challenging survival conditions. We further note that these data correlate with subtle changes in iPSC phenotype between cells grown on RDG-ELP *vs.* RGD-ELP substrates. iPSCs grown on RDG-ELP substrates appear to have a more rounded and less adherent morphology (Fig. 1) with higher overall YAP expression (Fig. 5), and they more robustly express protein markers of stemness (Fig. 3) and prevent aberrant gene expression of differentiation markers (Fig. 4). Thus, these results merit the further study of RDG-ELP substrates as a reproducible, animal-free culture surface for the biofabrication of potent iPSC-derived exosomes. Future work will require identification of the miRNA target and validation of these observations using *in vivo* preclinical models to verify potential clinical relevance.

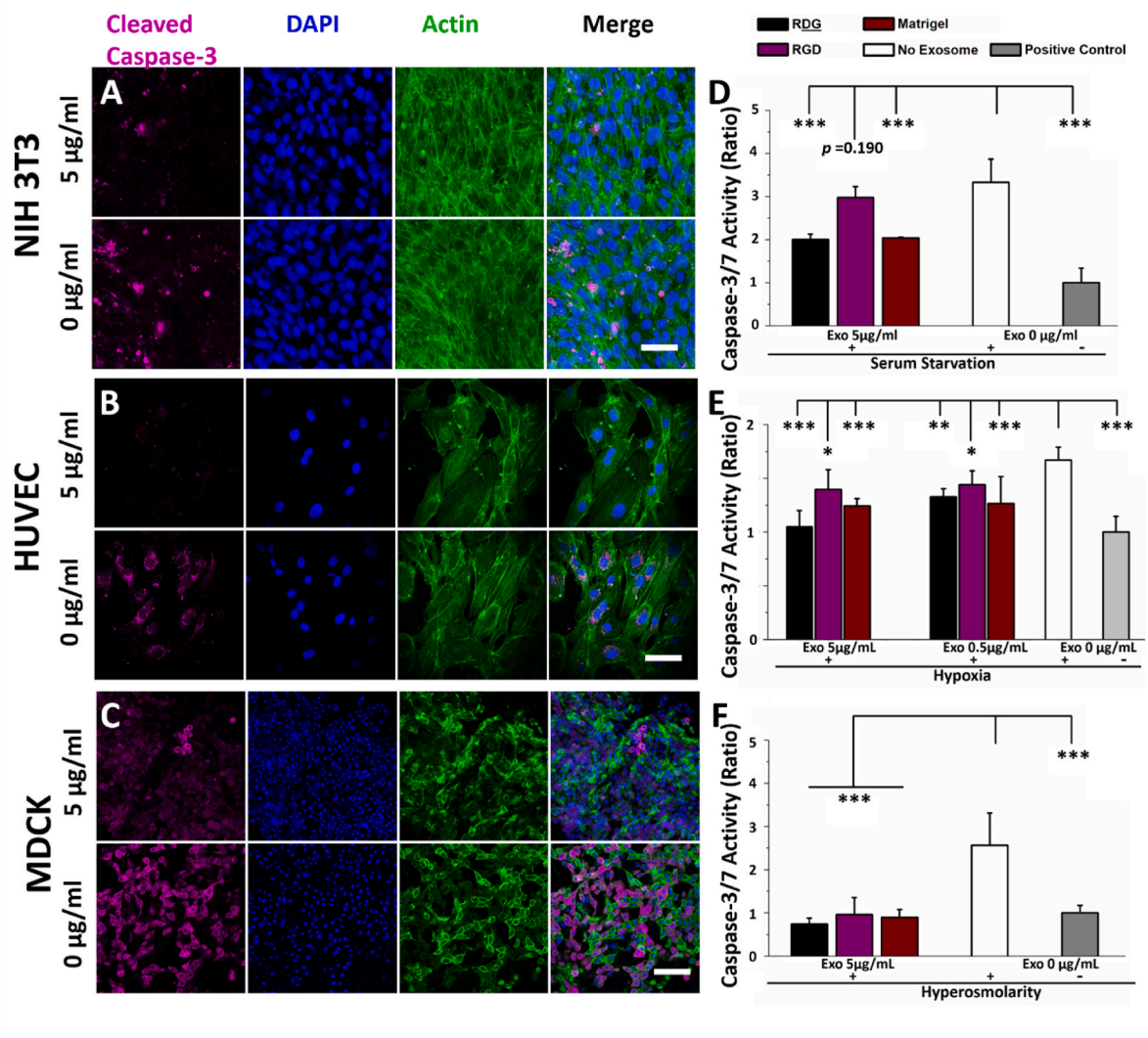

Fig. 10. Apoptotic rescue for three different cell challenge assays using exosomes from SCVI480 iPSCs. Evaluation of caspase activity by immunostaining for cleaved caspase-3 (A–C) and quantification with Apo-ONE® Homogeneous Caspase-3/7 assay (D–F) for NIH 3T3 fibroblasts exposed to serum starvation, HUVEC exposed to hypoxia, and MDCK exposed to hypertonic medium for 24 h, respectively. Scale bar = 50 µm $*p < 0.05$; $**p < 0.01$; $***p < 0.001$.

4. Conclusion

Exosomes have great future potential as cell-free therapies for regenerative medicine. To assist with the future scalable manufacturing of exosome therapies, reproducible and cell-free production protocols are required. Here we demonstrate that animal-free designer substrates can be developed using recombinant protein engineering methods to enable the production of iPSC-derived exosomes. In particular, ELP can be physically adsorbed to traditional tissue culture surfaces to create substrates for iPSC-derived exosome production. Molecular-level design choices for the ELP substrate, specifically the presence or absence of an integrin-adhesive RGD ligand, resulted in subtle differences in iPSC phenotype, which correlated with altered exosome potency. The RDG-ELP substrate significantly increased protein expression of the stemness markers OCT4 and SOX2 in two different iPSC lines compared to the RGD-ELP substrate. Exosomes produced by iPSCs grown on RGD-ELP substrates had reduced potency across three different mammalian cell challenge assays: serum starvation of murine fibroblasts, hypoxia of human endothelial cells, and hyperosmolarity of canine kidney cells. In contrast, exosomes produced on the RDG-ELP substrates had similar pro-survival effects to those produced using Matrigel across all three assays. Together, these data demonstrate that animal-free substrates can be designed for the robust bio-manufacturing of iPSC-derived, pro-survival exosomes.

Credit author statement

Chen-Hung Lee: Conceptualization, Writing – original draft, Visualization, Data curation, Investigation, Project administration. **Daniel Hunt**: Methodology, Validation, Software, Formal analysis. **Julien George Roth**: Formal analysis, Methodology, Software. **Ching-Chi Chiu:** Investigation, Validation. **Riley A. Suhar**: Software, Methodology. **Bauer L. LeSavage**: Methodology. **Alexis Jane Seymour**: Methodology. **Chris Lindsay**: Methodology. **Brad Krajina**: Methodology. **Yi-Tung Chen:** Investigation, Validation. **Kuo-Hsuan Chang:**Validation. **I-Chang Hsieh:** Funding acquisition. **Pao-Hsien, Chu:** Funding acquisition. **Ming-Shien Wen:** Funding acquisition. **Sarah C. Heilshorn**: Writing – review & editing, Visualization, Supervision, Project administration, Funding acquisition.

Declaration of competing interest

The authors declare that they have no known competing financial interests or personal relationships that could have appeared to influence the work reported in this paper.

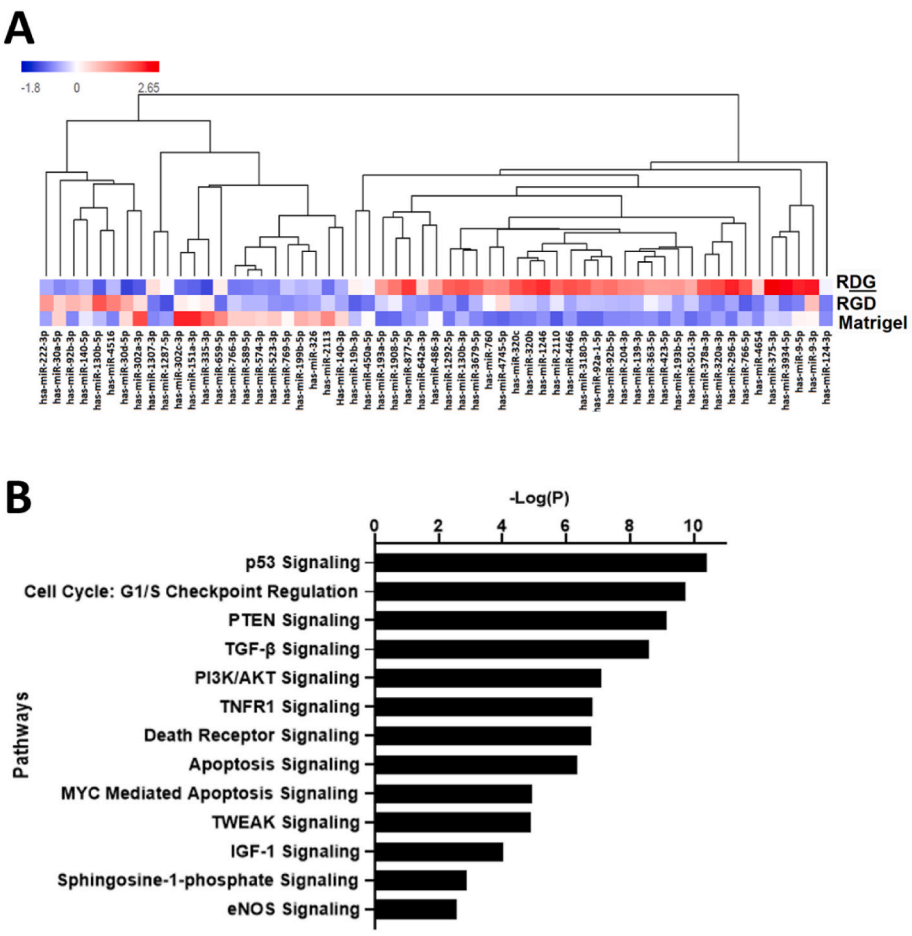

Fig. 11. Differentially expressed miRNAs in exosomes from iPSCs cultured on different substrates. (A) RNA sequencing was used to profile the exosomal miRNAs, and the expression values were indicated in shades of red or blue relative to the means of all corresponding values within individual groups on the heatmap. (B) Ingenuity Pathway Analysis was used to rank the pathways targeted by differentially expressed miRNAs from iPSC-derived exosomes produced on RDG-ELP substrates. (For interpretation of the references to colour in this figure legend, the reader is referred to the Web version of this article.)

Data availability

Data will be made available on request.

Acknowledgements

The authors would like to thank the National Science Council of Taiwan (MOST 109-2314-B-182A-035-MY3 and MOST 108-2221-E-182A-002to C–H L), Chang Gung Memorial Hospital (CMRPG3J1281, CMRPG3K1332, CMRPG3L1301, CORPG3M0151, and CMRPG3M1461 to C–H L), the National Science Foundation (DMR-1808415 to SCH), the National Institutes of Health (NIH) (R21 HL138042, R01 HL14271, and R01 EB027171 to SCH), NIH Training Grant in Biotechnology (T32-GM008412 to RAS) and the Stanford Lieberman Fellowship (to RAS) for financial support. JGR acknowledges support from an NSF Graduate Research Fellowship and a Smith Family Stanford Graduate Fellowship. B.L.L. thanks the Stanford Bio-X Bowes Graduate Fellowship program for financial support. The authors thank Prof. Joseph C. Wu (Stanford Cardiovascular Institute iPSC Biobank) and Prof. Theo Palmer (Stanford Neurosurgery Department) for human iPSC lines. The authors thank the Bioinformatics and Next-Generation Sequencing Core Laboratory, Molecular Medicine Research Center, Chang Gung University, Taiwan for technical support. The authors also thank Miss Ingrid Kuo and the Center for Big Data Analytics and Statistics (Grant CLRPG3D0049) at Chang Gung Memorial Hospital for creating schematic illustrations.

Appendix A. Supplementary data

Supplementary data to this article can be found online at https://doi.org/10.1016/j.biomaterials.2022.121864.

References

[1] S.K. Sanganalmath, R. Bolli, Cell therapy for heart failure: a comprehensive overview of experimental and clinical studies, current challenges, and future directions, Circ. Res. 113 (6) (2013) 810–834.
[2] P.S. Baker, G.C. Brown, Stem-cell therapy in retinal disease, Curr. Opin. Ophthalmol. 20 (3) (2009) 175–181.
[3] P. Martínez-Morales, A. Revilla, I. Ocana, C. Gonzalez, P. Sainz, D. McGuire, I. Liste, Progress in stem cell therapy for major human neurological disorders, Stem Cell Reviews and Reports 9 (5) (2013) 685–699.
[4] K. Takahashi, K. Tanabe, M. Ohnuki, M. Narita, T. Ichisaka, K. Tomoda, S. Yamanaka, Induction of pluripotent stem cells from adult human fibroblasts by defined factors, Cell 131 (5) (2007) 861–872.
[5] S.T. Rashid, G.J. Alexander, Induced pluripotent stem cells: from nobel prizes to clinical applications, J. Hepatol. 58 (3) (2013) 625–629.
[6] M. Stadtfeld, K. Hochedlinger, Induced pluripotency: history, mechanisms, and applications, Genes Dev. 24 (20) (2010) 2239–2263.
[7] K. Takahashi, S. Yamanaka, Induction of pluripotent stem cells from mouse embryonic and adult fibroblast cultures by defined factors, Cell 126 (4) (2006) 663–676.
[8] M. Adamiak, G. Cheng, S. Bobis-Wozowicz, L. Zhao, S. Kedracka-Krok, A. Samanta, E. Karnas, Y.-T. Xuan, B. Skupien-Rabian, X. Chen, Induced pluripotent stem cell (iPSC)–derived extracellular vesicles are safer and more effective for cardiac repair than iPSCs, Circ. Res. 122 (2) (2018) 296–309.
[9] J. Basu, J.W. Ludlow, Exosomes for repair, regeneration and rejuvenation, Expet Opin. Biol. Ther. 16 (4) (2016) 489–506.
[10] S. Kourembanas, Exosomes: vehicles of intercellular signaling, biomarkers, and vectors of cell therapy, Annu. Rev. Physiol. 77 (2015) 13–27.
[11] D.G. Phinney, M.F. Pittenger, Concise review: MSC-derived exosomes for cell-free therapy, Stem Cell. 35 (4) (2017) 851–858.
[12] L. Cheng, R.A. Sharples, B.J. Scicluna, A.F. Hill, Exosomes provide a protective and enriched source of miRNA for biomarker profiling compared to intracellular and cell-free blood, J. Extracell. Vesicles 3 (1) (2014), 23743.
[13] M. Aslam, R. Baveja, O.D. Liang, A. Fernandez-Gonzalez, C. Lee, S.A. Mitsialis, S. Kourembanas, Bone marrow stromal cells attenuate lung injury in a murine model of neonatal chronic lung disease, Am. J. Respir. Crit. Care Med. 180 (11) (2009) 1122–1130.

[14] T. Zhao, F. Sun, J. Liu, T. Ding, J. She, F. Mao, W. Xu, H. Qian, Y. Yan, Emerging role of mesenchymal stem cell-derived exosomes in regenerative medicine, Curr. Stem Cell Res. Ther. 14 (6) (2019) 482–494.
[15] J. Nussbaum, E. Minami, M.A. Laflamme, J.A. Virag, C.B. Ware, A. Masino, V. Muskheli, L. Pabon, H. Reinecke, C.E. Murry, Transplantation of undifferentiated murine embryonic stem cells in the heart: teratoma formation and immune response, Faseb. J. 21 (7) (2007) 1345–1357.
[16] N. Suzuki, S. Yamazaki, T. Yamaguchi, M. Okabe, H. Masaki, S. Takaki, M. Otsu, H. Nakauchi, Generation of engraftable hematopoietic stem cells from induced pluripotent stem cells by way of teratoma formation, Mol. Ther. 21 (7) (2013) 1424–1431.
[17] T.A. Prokhorova, L.M. Harkness, U. Frandsen, N. Ditzel, H.D. Schrøder, J.S. Burns, M. Kassem, Teratoma formation by human embryonic stem cells is site dependent and enhanced by the presence of Matrigel, Stem Cell. Dev. 18 (1) (2009) 47–54.
[18] Y. Li, S. Powell, E. Brunette, J. Lebkowski, R. Mandalam, Expansion of human embryonic stem cells in defined serum-free medium devoid of animal-derived products, Biotechnol. Bioeng. 91 (6) (2005) 688–698.
[19] C. Rao, T. Prodromakis, L. Kolker, U.A. Chaudhry, T. Trantidou, A. Sridhar, C. Weekes, P. Camelliti, S.E. Harding, A. Darzi, The effect of microgrooved culture substrates on calcium cycling of cardiac myocytes derived from human induced pluripotent stem cells, Biomaterials 34 (10) (2013) 2399–2411.
[20] Y.W. Chun, D.A. Balikov, T.K. Feaster, C.H. Williams, C.C. Sheng, J.-B. Lee, T. C. Boire, M.D. Neely, L.M. Bellan, K.C. Ess, Combinatorial polymer matrices enhance in vitro maturation of human induced pluripotent stem cell-derived cardiomyocytes, Biomaterials 67 (2015) 52–64.
[21] N. Javeed, D. Mukhopadhyay, Exosomes and their role in the micro-/macro-environment: a comprehensive review, Journal of Biomedical Research 31 (5) (2017) 386.
[22] Y. Zhang, J. Bi, J. Huang, Y. Tang, S. Du, P. Li, Exosome: a review of its classification, isolation techniques, storage, diagnostic and targeted therapy applications, Int. J. Nanomed. 15 (2020) 6917.
[23] M. Akbarzadeh, R. Rahbarghazi, E. Nabat, A.A. Movassaghpour, D. Shanehbandi, B.F.A. Maragheh, D. Matluobi, B. Barazvan, M. Kazemi, N. Samadi, The impact of different extracellular matrices on melatonin effect in proliferation and stemness properties of ovarian cancer cells, Biomed. Pharmacother. 87 (2017) 288–295.
[24] J. Zhang, J.H.-C. Wang, Human tendon stem cells better maintain their stemness in hypoxic culture conditions, PLoS One 8 (4) (2013).
[25] T. Umezu, K. Ohyashiki, M. Kuroda, J. Ohyashiki, Leukemia cell to endothelial cell communication via exosomal miRNAs, Oncogene 32 (22) (2013) 2747–2755.
[26] M. Mineo, S.H. Garfield, S. Taverna, A. Flugy, G. De Leo, R. Alessandro, E.C. Kohn, Exosomes released by K562 chronic myeloid leukemia cells promote angiogenesis in a Src-dependent fashion, Angiogenesis 15 (1) (2012) 33–45.
[27] C.S. Hughes, L.M. Postovit, G.A. Lajoie, Matrigel: a complex protein mixture required for optimal growth of cell culture, Proteomics 10 (9) (2010) 1886–1890.
[28] H.K. Kleinman, M.L. McGarvey, L.A. Liotta, P.G. Robey, K. Tryggvason, G. R. Martin, Isolation and characterization of type IV procollagen, laminin, and heparan sulfate proteoglycan from the EHS sarcoma, Biochemistry 21 (24) (1982) 6188–6193.
[29] D.W. Urry, Free energy transduction in polypeptides and proteins based on inverse temperature transitions, Prog. Biophys. Mol. Biol. 57 (1) (1992) 23–57.
[30] D.W. Urry, T.M. Parker, M.C. Reid, D.C. Gowda, Biocompatibility of the bioelastic materials, poly (GVGVP) and its γ-irradiation cross-linked matrix: summary of generic biological test results, J. Bioact. Compat Polym. 6 (3) (1991) 263–282.
[31] S.R. MacEwan, A. Chilkoti, Elastin-like polypeptides: biomedical applications of tunable biopolymers, Peptide Science: Original Research on Biomolecules 94 (1) (2010) 60–77.
[32] D.L. Nettles, A. Chilkoti, L.A. Setton, Applications of elastin-like polypeptides in tissue engineering, Adv. Drug Deliv. Rev. 62 (15) (2010) 1479–1485.
[33] E. Ruoslahti, M.D. Pierschbacher, New perspectives in cell adhesion: RGD and integrins, Science 238 (4826) (1987) 491–497.
[34] E. Ruoslahti, RGD and other recognition sequences for integrins, Annu. Rev. Cell Dev. Biol. 12 (1) (1996) 697–715.
[35] T.J. Rowland, L.M. Miller, A.J. Blaschke, E.L. Doss, A.J. Bonham, S.T. Hikita, L. V. Johnson, D.O. Clegg, Roles of integrins in human induced pluripotent stem cell growth on matrigel and vitronectin, Stem Cell. Dev. 19 (8) (2009) 1231–1240.
[36] T. Yu, S. Miyagawa, K. Miki, A. Saito, S. Fukushima, T. Higuchi, M. Kawamura, T. Kawamura, E. Ito, N. Kawaguchi, In vivo differentiation of induced pluripotent stem cell-derived cardiomyocytes, Circ. J. 77 (5) (2013) 1297–1306.
[37] T.T. Lee, J.R. García, J.I. Paez, A. Singh, E.A. Phelps, S. Weis, Z. Shafiq, A. Shekaran, A. Del Campo, A.J. García, Light-triggered in vivo activation of adhesive peptides regulates cell adhesion, inflammation and vascularization of biomaterials, Nat. Mater. 14 (3) (2015) 352–360.
[38] K.R. Legate, S.A. Wickström, R. Fässler, Genetic and cell biological analysis of integrin outside-in signaling, Genes Dev. 23 (4) (2009) 397–418.
[39] B.L. LeSavage, N.A. Suhar, C.M. Madl, S.C. Heilshorn, Production of elastin-like protein hydrogels for encapsulation and immunostaining of cells in 3D, JoVE (135) (2018), e57739.
[40] K.S. Straley, S.C. Heilshorn, Independent tuning of multiple biomaterial properties using protein engineering, Soft Matter 5 (1) (2009) 114–124.
[41] R.L. DiMarco, S.C. Heilshorn, Multifunctional materials through modular protein engineering, Adv. Mater. 24 (29) (2012) 3923–3940.
[42] J. Raphel, A. Parisi-Amon, S.C. Heilshorn, Photoreactive elastin-like proteins for use as versatile bioactive materials and surface coatings, J. Mater. Chem. 22 (37) (2012) 19429–19437.
[43] P.L. Benitez, J.A. Sweet, H. Fink, K.P. Chennazhi, S.V. Nair, A. Enejder, S. C. Heilshorn, Sequence-specific crosslinking of electrospun, elastin-like protein preserves bioactivity and native-like mechanics, Advanced Healthcare Materials 2 (1) (2013) 114–118.
[44] X. Kang, Y. Zhao, G. Van Arsdell, S.F. Nelson, M. Touma, Ppp1r1b-lncRNA inhibits PRC2 at myogenic regulatory genes to promote cardiac and skeletal muscle development in mouse and human, RNA 26 (4) (2020) 481–491.
[45] J.G. Roth, K.L. Muench, A. Asokan, V.M. Mallett, H. Gai, Y. Verma, S. Weber, C. Charlton, J.L. Fowler, K.M. Loh, 2 microdeletion imparts transcriptional alterations in human iPSC-derived models of early neural development, 16p.11, Elife 9 (2020), e58178.
[46] C.Y. Huang, M.W. Nicholson, J.Y. Wang, C.Y. Ting, M.H. Tsai, Y.C. Cheng, C.L. Liu, D.Z. Chan, Y.C. Lee, C.C. Hsu, Population-based high-throughput toxicity screen of human iPSC-derived cardiomyocytes and neurons, Cell Rep. 39 (1) (2022), 110643.
[47] A.-K. Ludwig, K. De Miroschedji, T.R. Doeppner, V. Börger, J. Ruesing, V. Rebmann, S. Durst, S. Jansen, M. Bremer, E. Behrmann, Precipitation with polyethylene glycol followed by washing and pelleting by ultracentrifugation enriches extracellular vesicles from tissue culture supernatants in small and large scales, J. Extracell. Vesicles 7 (1) (2018), 1528109.
[48] H. Wang, L. Cai, A. Paul, A. Enejder, S.C. Heilshorn, Hybrid elastin-like polypeptide–polyethylene glycol (ELP-PEG) hydrogels with improved transparency and independent control of matrix mechanics and cell ligand density, Biomacromolecules 15 (9) (2014) 3421–3428.
[49] K.J. Lampe, A.L. Antaris, S.C. Heilshorn, Design of three-dimensional engineered protein hydrogels for tailored control of neurite growth, Acta Biomater. 9 (3) (2013) 5590–5599.
[50] C. Xu, M.S. Inokuma, J. Denham, K. Golds, P. Kundu, J.D. Gold, M.K. Carpenter, Feeder-free growth of undifferentiated human embryonic stem cells, Nat. Biotechnol. 19 (10) (2001) 971–974.
[51] L. Zhou, W. Wang, Y. Liu, J.F. de Castro, T. Ezashi, B.P.V. Telugu, R.M. Roberts, H. J. Kaplan, D.C. Dean, Differentiation of induced pluripotent stem cells of swine into rod photoreceptors and their integration into the retina, Stem Cell. 29 (6) (2011) 972–980.
[52] E. Garreta, P. Prado, C. Tarantino, R. Oria, L. Fanlo, E. Martí, D. Zalvidea, X. Trepat, P. Roca-Cusachs, A. Gavaldà-Navarro, Fine tuning the extracellular environment accelerates the derivation of kidney organoids from human pluripotent stem cells, Nat. Mater. 18 (4) (2019) 397–405.
[53] T. Lei, H.-P. Hohn, R. Behr, H.-W. Denker, Influences of extracellular matrix and of conditioned media on differentiation and invasiveness of trophoblast stem cells, Placenta 28 (1) (2007) 14–21.
[54] R. Wang, K.B. McCauley, D.N. Kotton, F. Hawkins, Differentiation of human airway-organoids from induced pluripotent stem cells (iPSCs), Methods in Cell Biology, Elsevier2020, pp. 95-114.
[55] T. Miyazaki, S. Futaki, H. Suemori, Y. Taniguchi, M. Yamada, M. Kawasaki, M. Hayashi, H. Kumagai, N. Nakatsuji, K. Sekiguchi, Laminin E8 fragments support efficient adhesion and expansion of dissociated human pluripotent stem cells, Nat. Commun. 3 (1) (2012) 1–11.
[56] Y. Liu, A. Beyer, R. Aebersold, On the dependency of cellular protein levels on mRNA abundance, Cell 165 (3) (2016) 535–550.
[57] Z. Cheng, G. Teo, S. Krueger, T.M. Rock, H.W. Koh, H. Choi, C. Vogel, Differential dynamics of the mammalian mRNA and protein expression response to misfolding stress, Mol. Syst. Biol. 12 (1) (2016) 855.
[58] Y.-L. Kuang, A. Munoz, G. Nalula, K.E. Santostefano, V. Sanghez, G. Sanchez, N. Terada, A.N. Mattis, M. Iacovino, C. Iribarren, Evaluation of commonly used ectoderm markers in iPSC trilineage differentiation, Stem Cell Res. 37 (2019), 101434.
[59] D. Lenz, C. Staufner, S. Waechter, M. Hagedorn, J. Ebersold, G. Goehring, S. Koelker, G.F. Hoffmann, S. Jung-Klawitter, Generation of an induced pluripotent stem cell (iPSC) line, DHMCi005-A, from a patient with CALFAN syndrome due to mutations in SCYL1, Stem Cell Res. 37 (2019), 101428.
[60] M.A. Wozniak, K. Modzelewska, L. Kwong, P.J. Keely, Focal adhesion regulation of cell behavior, Biochim. Biophys. Acta Mol. Cell Res. 1692 (2–3) (2004) 103–119.
[61] G. Nardone, J. Oliver-De La Cruz, J. Vrbsky, C. Martini, J. Pribyl, P. Skládal, M. Pešl, G. Caluori, S. Pagliari, F. Martino, YAP regulates cell mechanics by controlling focal adhesion assembly, Nat. Commun. 8 (2017), 15321.
[62] Y. Wang, A. Yu, F.-X. Yu, The Hippo pathway in tissue homeostasis and regeneration, Protein & Cell 8 (5) (2017) 349–359.
[63] L. Cairns, T. Tran, J.M. Kavran, Structural insights into the regulation of hippo signaling, ACS Chem. Biol. 12 (3) (2017) 601–610.
[64] Z. Meng, Y. Qiu, K.C. Lin, A. Kumar, J.K. Placone, C. Fang, K.-C. Wang, S. Lu, M. Pan, A.W. Hong, RAP2 mediates mechanoresponses of the Hippo pathway, Nature 560 (7720) (2018) 655–660.
[65] S. Rammensee, M.S. Kang, K. Georgiou, S. Kumar, D.V. Schaffer, Dynamics of mechanosensitive neural stem cell differentiation, Stem Cell. 35 (2) (2017) 497–506.
[66] M. Bachmann, S. Kukkurainen, V.P. Hytönen, B. Wehrle-Haller, Cell adhesion by integrins, Physiol. Rev. 99 (4) (2019) 1655–1699.
[67] A. Das, R.S. Fischer, D. Pan, C.M. Waterman, YAP nuclear localization in the absence of cell-cell contact is mediated by a filamentous actin-dependent, myosin II-and phospho-YAP-independent pathway during extracellular matrix mechanosensing, J. Biol. Chem. 291 (12) (2016) 6096–6110.
[68] M. Barczyk, S. Carracedo, D. Gullberg, Integrins, Cell and Tissue Research 339 (1) (2010) 269–280.
[69] M.Y. Konoshenko, E.A. Lekchnov, A.V. Vlassov, P.P. Laktionov, Isolation of extracellular vesicles: general methodologies and latest trends, BioMed Res. Int. (2018).

[70] K. Boriachek, M.N. Islam, A. Möller, C. Salomon, N.T. Nguyen, M.S.A. Hossain, Y. Yamauchi, M.J. Shiddiky, Biological functions and current advances in isolation and detection strategies for exosome nanovesicles, Small 14 (6) (2018), 1702153.
[71] J. Van Deun, P. Mestdagh, R. Sormunen, V. Cocquyt, K. Vermaelen, J. Vandesompele, M. Bracke, O. De Wever, A. Hendrix, The impact of disparate isolation methods for extracellular vesicles on downstream RNA profiling, J. Extracell. Vesicles 3 (1) (2014), 24858.
[72] D.D. Taylor, S. Shah, Methods of isolating extracellular vesicles impact down-stream analyses of their cargoes, Methods 87 (2015) 3–10.
[73] M. Colombo, G. Raposo, C. Théry, Biogenesis, secretion, and intercellular interactions of exosomes and other extracellular vesicles, Annu. Rev. Cell Dev. Biol. 30 (2014) 255–289.
[74] A. Bobrie, M. Colombo, G. Raposo, C. Théry, Exosome secretion: molecular mechanisms and roles in immune responses, Traffic 12 (12) (2011) 1659–1668.
[75] J. Lötvall, A.F. Hill, F. Hochberg, E.I. Buzás, D. Di Vizio, C. Gardiner, Y.S. Gho, I. V. Kurochkin, S. Mathivanan, P. Quesenberry, Minimal Experimental Requirements for Definition of Extracellular Vesicles and Their Functions: a Position Statement from the International Society for Extracellular Vesicles, Taylor & Francis, 2014.
[76] L.M. Doyle, M.Z. Wang, Overview of extracellular vesicles, their origin, composition, purpose, and methods for exosome isolation and analysis, Cells 8 (7) (2019) 727.
[77] C. Théry, K.W. Witwer, E. Aikawa, M.J. Alcaraz, J.D. Anderson, R. Andriantsitohaina, A. Antoniou, T. Arab, F. Archer, G.K. Atkin-Smith, Minimal information for studies of extracellular vesicles 2018 (MISEV2018): a position statement of the International Society for Extracellular Vesicles and update of the MISEV2014 guidelines, J. Extracell. Vesicles 7 (1) (2018), 1535750.
[78] X. Wang, W. Huang, G. Liu, W. Cai, R.W. Millard, Y. Wang, J. Chang, T. Peng, G.-C. Fan, Cardiomyocytes mediate anti-angiogenesis in type 2 diabetic rats through the exosomal transfer of miR-320 into endothelial cells, J. Mol. Cell. Cardiol. 74 (2014) 139–150.
[79] R. Kishore, M. Khan, More than tiny sacks: stem cell exosomes as cell-free modality for cardiac repair, Circ. Res. 118 (2) (2016) 330–343.
[80] M. Ailenberg, M. Silverman, Cytochalasin D disruption of actin filaments in 3T3 cells produces an anti-apoptotic response by activating gelatinase A extracellularly and initiating intracellular survival signals, Biochim. Biophys. Acta Mol. Cell Res. 1593 (2–3) (2003) 249–258.
[81] Q.-B. She, J.J. Mukherjee, T. Chung, Z. Kiss, Placental alkaline phosphatase, insulin, and adenine nucleotides or adenosine synergistically promote long-term survival of serum-starved mouse embryo and human fetus fibroblasts, Cell. Signal. 12 (9–10) (2000) 659–665.
[82] N. Ludwig, T.L. Whiteside, Potential roles of tumor-derived exosomes in angiogenesis, Expert Opin. Ther. Targets 22 (5) (2018) 409–417.
[83] I. Giusti, S. Delle Monache, M. Di Francesco, P. Sanità, S. D'Ascenzo, G.L. Gravina, C. Festuccia, V. Dolo, From glioblastoma to endothelial cells through extracellular vesicles: messages for angiogenesis, Tumor Biol. 37 (9) (2016) 12743–12753.
[84] I. Hizoh, J. Sträter, C. Schick, W. Kübler, C. Haller, Radiocontrast-induced DNA fragmentation of renal tubular cells in vitro: role of hypertonicity, Nephrology, dialysis, transplantation: official publication of the European Dialysis and Transplant Association-European, Renal Association 13 (4) (1998) 911–918.
[85] B.C. Santos, A. Chevaile, M.-J. Hébert, J. Zagajeski, S.R. Gullans, A combination of NaCl and urea enhances survival of IMCD cells to hyperosmolality, Am. J. Physiol. Ren. Physiol. 274 (6) (1998) F1167–F1173.
[86] T. Ma, B. Fu, X. Yang, Y. Xiao, M. Pan, Adipose mesenchymal stem cell-derived exosomes promote cell proliferation, migration, and inhibit cell apoptosis via Wnt/β-catenin signaling in cutaneous wound healing, J. Cell. Biochem. 120 (6) (2019) 10847–10854.
[87] Y. Bai, X.-l. Yan, J. Ren, Q. Zeng, X.-d. Li, X.-t. Pei, Y. Han, Adipose mesenchymal stem cell-derived exosomes stimulated by hydrogen peroxide enhanced skin flap recovery in ischemia-reperfusion injury, Biochem. Biophys. Res. Commun. 500 (2) (2018) 310–317.
[88] Y. Li, J. Jiang, W. Liu, H. Wang, L. Zhao, S. Liu, P. Li, S. Zhang, C. Sun, Y. Wu, microRNA-378 promotes autophagy and inhibits apoptosis in skeletal muscle, Proc. Natl. Acad. Sci. USA 115 (46) (2018) E10849–E10858.